ACS APPLIED MATERIALS & INTERFACES

Research Article

www.acsami.org

# Comparative Study of Structure and Permeability of Porous Oxide Films on Aluminum Obtained by Single- and Two-Step Anodization

Dmitrii I. Petukhov,[†,‡,*] Kirill S. Napolskii,[†,‡] Mikhail V. Berekchiyan,[†] Alexander G. Lebedev,[§] and Andrey A. Eliseev[†,‡]

[†]Department of Materials Science, [‡]Department of Chemistry, and [§]Department of Mechanics and Mathematics, Lomonosov Moscow State University, Leninskie Gory 119991, Moscow, Russia

**ABSTRACT:** A comparative study of the structure and transport properties of porous aluminum oxide films obtained by single- and two-step anodization was carried out. It is shown that the oxidation regime significantly affect the number of dead-ended channels, which results in more than twice the variation in membrane permeability. The effect is explained by multiple branching of channels on the initial stages of organization of the porous structure. Branching also occurs on later stages governing mass transport properties of porous anodic alumina films. A model describing transport properties of anodic aluminum oxide membranes based on pore branching on domain boundaries was suggested to fit experimental results of permeance of membranes obtained by both single- and two-step anodization.

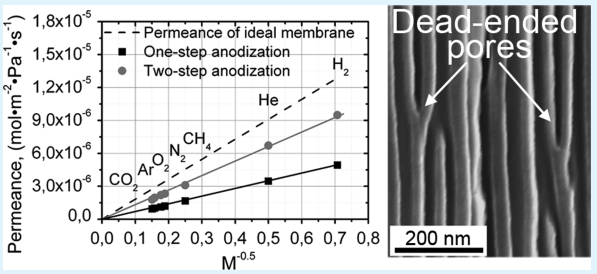


**KEYWORDS:** *anodic aluminum oxide membranes, two-step anodization, mass-transport, self-ordering, branched channels, dead-ended channels*

## INTRODUCTION

The process of anodic oxidation of aluminum to form corrosion protective or adhesive coatings has been used extensively in industry for about a century.[1] In the last few decades, a number of hi-tech applications of anodic aluminum oxide (AAO) have arisen because of the discovery of anodization conditions leading to the formation of self-ordered porous structures with narrow pore size distribution.[2,3] It is generally accepted and proved[4,5] experimentally that a highly ordered porous structure can be obtained by the two-step anodic oxidation of aluminum. It results in better ordering and circularity of the pores.[6] However, the benefits of a two-step process over a single-step anodization are not well understood, except for a perfect view of anodic films. Only a few studies assert the importance of using long-term oxidation regimes or nanoimprint of the aluminum surface prior to anodization, for the improvement of functional properties of AAO-based materials.[7−9] In contrast, a number of works devoted to practical functions of AAO including membranes,[10,11] templating of nanowires,[12] AAO applications in sensors,[13] or supercapacitors[14] utilize a single-step oxidation procedure.

The growth of anodic film on aluminum is known to start with a stage of pore nucleation on concavities on the aluminum surface. Then numerous pore nuclei compete to turn into the stable pore growth regime. This stage is characterized by a decrease in pore density and multiple formation of dead-ended channels. If anodization is performed under self-ordered conditions (e.g., at 25 V in 0.3 M $H_2SO_4$ or at 40 V in 0.3 M $H_2C_2O_4$), the evolution of the porous structure involves a redistribution of channels to form the regions with a regular pore arrangement (the domains). Further transformation of the porous structure takes place mostly on the domain boundaries, where one pore has an opportunity to split enlarging the area of hexagonally ordered domain with optimal orientation, while the neighboring pore has to stop growing.[15] These processes lead to the formation of a large number of dead-ended channels, which negatively affects the through porosity of AAO membranes.

As well as prepatterning of the aluminum surface by nanoimprint lithography, two-step anodization has been developed to increase pore ordering in AAO films by creating a well-defined network of concavities or defects, which can serve as pore nuclei in the first stage of anodization. This obviously decreases the number of dead-ended pores and increases the through porosity of anodic films.

Despite a general simplicity of the growth model any quantitative information on the through porosity of anodic films, formed by single- and two-step anodization is absent in the literature, while this parameter has a major implication for any mass-transport applications or pore loading factors achievable by electrochemical or chemical methods.[16−18]

Thus, in the present study, we provide a comparison of the structure of anodic films formed by single- and two-step anodization, from a practical point of view. A detailed examination of mass-transport characteristics of anodic alumina membranes and through porosity is provided.

**Received:** April 29, 2013
**Accepted:** July 23, 2013
**Published:** July 23, 2013

   dx.doi.org/10.1021/am401585q | *ACS Appl. Mater. Interfaces* 2013, 5, 7819−7824

## EXPERIMENTAL SECTION

**Sample Preparation.** Prior to anodization, aluminum foils (99.999%, 0.5 mm thick, Goodfellow) were annealed at 450 °C for 24h in air, in order to remove any mechanical stress, and to enhance the grain size in the metal. Subsequently, the Al plates were polished electrochemically in 184 g/L $CrO_3$ + 836 mL/L $H_3PO_4$ electrolyte in pulsed mode (pulse duration, 3 s; interpulse spacing, 40 s; current density, 0.65 A/cm$^2$; pulse number, 40),[19,20] and cleaned repeatedly with deionized water and acetone.

The anodization was carried out in a two-electrode cell (similar to that described in ref 7.) in 0.3 M $H_2C_2O_4$ (98%, Aldrich) at a constant voltage of 40 V. The electrolyte was pumped through the two-electrode cell by a peristaltic pump, and its temperature was kept constant (2 °C) during anodization. The films, with thicknesses ranging from 70 to 315 $\mu$m, were obtained by controlling total electric quantity and assuming current efficiency of 90%.[21]

Two-step anodization was carried out by the dissolution of the anodic oxide layer formed on preanodized aluminum, followed by a second anodization step performed under the same conditions. Preanodization duration ($t_1$) varied from 3 to 48 h (corresponding to porous film thickness of 10 − 100 $\mu$m). Selective etching of the anodic film was performed in 35 mL/L $H_3PO_4$ + 20 g/L $CrO_3$ solution at 60 °C. The duration of the second step of the anodization ($t_2$) was varied from 20 to 120 h. AAO films with an area of about 1.1 cm$^2$, and thicknesses from 40 to 270 $\mu$m, were obtained by coulometric control.

The oxide films were separated from the metallic substrates by selective metal dissolution in 0.5 M $CuCl_2$ in 5 vol % HCl. Subsequently, the pore bottoms were opened by chemical etching in 5 vol % $H_3PO_4$ aqueous solution at 60 °C with electrochemical detection of the pore opening point.[22,23] The average time of etching was about 5 min.

**Sample Characterization.** Scanning electron microscopy (SEM) images were recorded on a Supra 50VP instrument (LEO). The statistical analysis of obtained micrographs for determination of pore size distribution, porosity and pore density was performed using ImageJ software. The same procedure for analysis of the pore diameter was used in ref 24. Pore density on the surfaces of AAO was determined after converting the grayscale micrograph into a binary (black and white) image. Pore density was calculated as a ratio between the number of black regions appropriate to pores and area of micrograph in square micrometers. Permeabilities of individual gases ($H_2$, He, $CH_4$, $N_2$, $O_2$, Ar, $CO_2$) through the membranes were measured at room temperature in steady-state experiments, with the permeation cell used in our previous work.[21]

## RESULTS AND DISCUSSION

The initial pore arrangement on the top side of an anodic film, obtained by single-step anodization, is completely irregular (Figure 1a) owing to the quasi-random nucleation of pores on the metal surface. During the anodization, the pores organize gradually into a hexagonal close-packed array, which is well illustrated by the bottom views of the anodic films after removal of the barrier layer by chemical etching (Figure 1b, d). Self-organization of the porous structure is accompanied by the reduction in pore density from ~180 ± 10 pores/$\mu$m$^2$ on the top alumina surface (Figure 1a) to ~105 ± 5 pores/$\mu$m$^2$ at the bottom surface of the membrane anodized for 48 h (Figure 1b). This obviously leads to the formation of blocked channels.

The anodic film/aluminum interface, formed during anodization in the dissolving electrolytes, is known to possess a regular relief, replicating the form and arrangement of the pores' bottoms in the anodic film. Selective dissolution of the porous layer preserves the relief of the metal, with a regular arrangement of concavities on the surface. Those serve further as pore nucleation centers in the course of the second anodization. Thus the anodic alumina films obtained by two-step anodization have a hexagonal arrangement of channels on both the top and the bottom sides (Figure 1c, d) with nearly the same pore density (105 ± 5 pores/$\mu$m$^2$). However, a careful analysis of cross-sectional images of AAO films (Figure 1e) illustrates the presence of dead-ended channels also in AAO membranes obtained by the two-step anodization technique. According to earlier studies, the termination of channels occurs during their self-organization on domain boundaries, where the surrounding of the pores is far from the hexagonal.[15] The process involves the movement of domain boundaries by the termination of a channel on the edge of a decreasing domain, and the branching of a neighboring pore into two channels inside the growing domain.

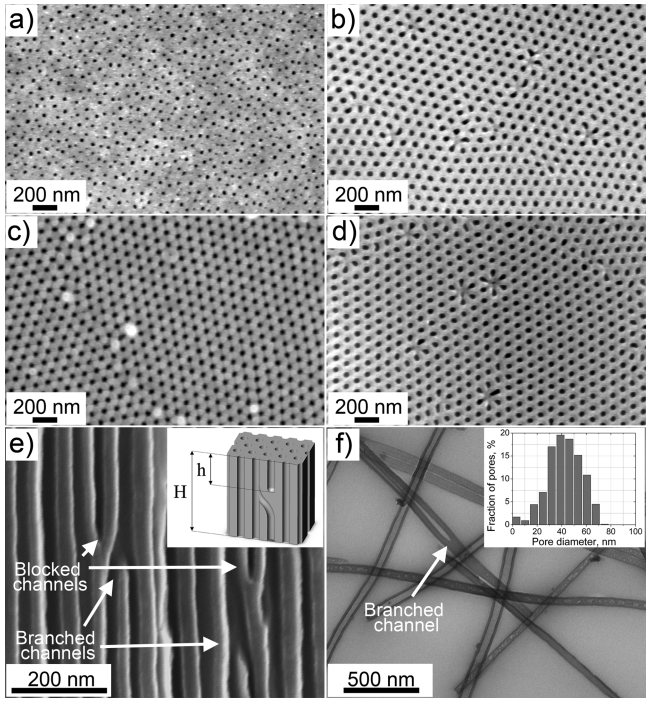


**Figure 1.** Morphology of anodic alumina membranes: (a) top view and (b) bottom view SEM images of oxide film prepared by single-step anodization; (c) top side and (d) bottom side of oxide film prepared by two-step anodization. (e) Cross-sectional micrograph of AAO porous structure. Dead-ended and branched pores are marked by arrows. The inset is a scheme of coexistence of branched and dead-ended pores in the structure of the anodic alumina film. (f) Typical TEM image of templated carbon nanotubes inside the pores of the anodic alumina membrane. The inset is a pore size distribution obtained by Barrett–Joyner–Halenda processing of capillary $N_2$ absorption data from AAO membrane.

Obviously, the aforementioned dead-ended pores in the anodic alumina film lead to a decrease in mass transport through the membrane. According to Fick's law, the permeance of the branch pore, split from the main straight channel at depth $h$ (see inset in Figure 1e), is given by:

$$p_{\text{branch}} = p_{\text{ideal}} \frac{(H-h)}{(H+h)} = \frac{F(H-h)}{(H+h)H} \quad (1)$$

where $p_{\text{ideal}}$ is permeance of a single straight pore, $F$ is permeability, and $H$ is the total film thickness. One can easily see that if pore termination occurs on the upper side of the membrane ($h \to 0$) the permeance of the porous system does not change significantly, while each termination close to the bottom side of membrane ($h \to H$) annuls the permeance of

the pore branch and decreases the total permeance of the porous membrane on $p_{ideal}$.

One can expect that the number of blocked channels would decrease substantially with an increase of pore ordering in the film. To provide a comparison of the transport properties, we took the gas permeance measurements through the membranes of the same thickness (100 $\mu$m), obtained by single- and two-step anodization (Figure 2). For both membranes, the

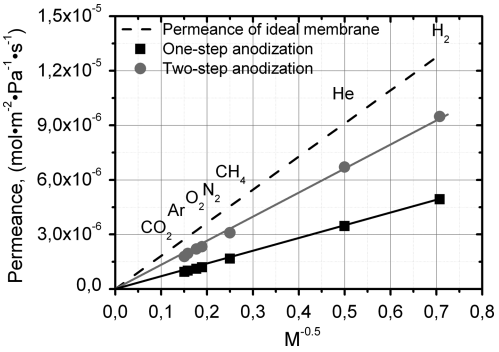


**Figure 2.** Permeance of different gases plotted against the inverse square root of their molecular weights for 100 $\mu$m thick membranes obtained by single- (black squares) and two-step (gray circles) anodization. Theoretical permeance for membrane without dead-ended pores is shown by dashed black line.

permeance is inversely proportional to the square root of the molecular weight of permeate gas, proving that the diffusion mechanism is Knudsen flow. However, the absolute permeation values were found to be nearly twice those for the membrane obtained by two-step anodization ($t_1$ = 48 h), as compared with the porous film prepared by the single-step technique. Moreover, both membranes illustrate a substantial permeance decrease, compared to theoretical Knusden permeance values, calculated for a 100 $\mu$m thick membrane with pore diameter of 40 nm and interpore distance of 104 nm.[10]

One should note that the real AAO samples possess ~30% dispersion of pore sizes due to native distribution of pore diameters and pore broadening near the top surface (as obtained by Barrett–Joyner–Halenda processing of capillary $N_2$ absorption data, see inset in Figure 1f). The permeance of such membrane can be estimated as a convolution product of permeance for membrane having experimental diameter distribution (at constant pore diameter along the channel) and the one having variable diameter along the channels.[10] The resulting value coincides with that obtained by a simple estimation with Knudsen flow model for 40 nm mean diameter of the pores with an accuracy of 10%, which is within the limits of permeability measurement errors. Therefore, to simplify the calculations hereafter, we used a constant diameter of the pores of 40 nm.

As all the membranes exhibit Knudsen diffusion mechanism, we took an average of the values of membrane permeance. All the permeances $P_{40}$ reported below in the paper were averaged over 7 individual gases, and renormalized for gas with molecular weight of 40 g/mol

$$P_{40} = \frac{1}{\sqrt{40}} \sum_{i=1}^{7} P_i \sqrt{M_i} \tag{2}$$

where $P_i$ is membrane permeance for gas with molecular weight $M_i$.

To trace the change in AAO membrane permeability with pore ordering, we performed permeance measurements for membranes of different thickness, ranging from 40 to 315 $\mu$m (Figure 3a). Assuming no variation in diameter of AAO channels with membrane thickness, the difference between experimental and theoretical permeances corresponds to the number of blocked channels, while the permeance change with membrane thickness reflects the distribution of dead-ended channels with anodization duration (or depth). For convenience the relative permeance of the membrane was introduced as

$$\eta = \frac{P_{40}}{P_{ideal}} \tag{3}$$

where $P_{ideal}$ is the theoretical value calculated by Knudsen equation, for gas with molecular weight of 40 g/mol. For all the obtained membranes, the relative permeance was found to be significantly below 1, which can be ascribed to the large number of blocked channels in the films' structure (Figure 1e). Moreover, the membranes obtained by single-step anodization demonstrate a substantial decrease in relative permeance at low thicknesses. This indicates that numerous blocking of channels occurs at the initial stages of anodization, which coincides well with the top views of the anodic aluminum films (Figure 1a,c).

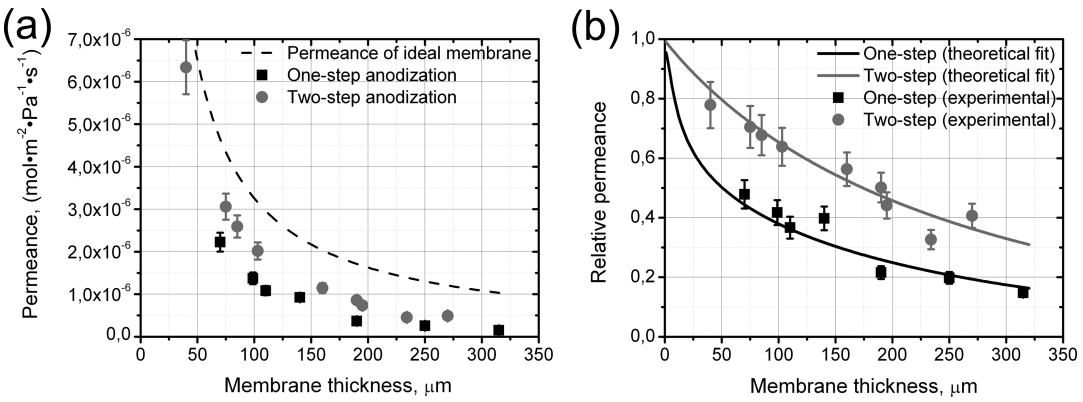


**Figure 3.** (a) Dependence of permeance on membrane thickness for ideal membranes with straight pores (dashed black line), membranes obtained by single- (black squares) and two-step (gray circles) anodization techniques. (b) Dependence of relative permeance of membranes synthesized by single- (black squares) and two-step (gray circles) anodization on membrane thickness vs. numerical calculations (solid lines).

To provide a quantitative description of the pore termination process, and the difference in permeance of membranes obtained by single- and two-step anodization, the kinetics of pore ordering was analyzed. Numerical simulations of pore ordering were carried out using the modified model suggested in ref 15. In brief, the model assumes a pore domains' growth mechanism, with probabilistic termination of pores on domain boundaries during their movement. The speed of domain boundary movement is assumed to be proportional to the difference of oxidation rates in neighboring domains, depending on pore system orientation toward crystallographic axes of aluminum,[25] and having Gaussian distribution around optimal orientation

$$U(\varphi) = U_0 + ke^{-(\varphi-\varphi_{max})^2/2\sigma^2} \quad (4)$$

where $U_0$ is a constant, depending on anodization conditions (i.e., voltage, temperature, electrolyte composition, etc.), $k$ is scaling factor, $\varphi$ is in-plane orientation of the domain ($0 \le \varphi < \pi/3$), $\varphi_{max}$ corresponds to an "optimal" in-plane orientation, and $\sigma$ is a standard deviation. According to ref 15, the experimental results for the case of anodic oxidation of aluminum at 40 V are best fitted with $\sigma \approx 30°$.

Under the condition of linear relation between oxidation rate and domain boundary movement, the domain growth rate at a certain time step of anodic oxidation complies with the relation

$$\Delta S_i(t) = \frac{\Delta t}{\gamma} \sum_{j=1, j\neq i}^{N} \left[ (U_{rnd} + U_i - U_j) \frac{L_i(t)L_j(t)}{L(t)} \right] \quad (5)$$

where $\gamma$ is a correlation coefficient connecting oxidation rate and the domain boundary movement speed, $N$ is the total number of domains, $U_i$ and $U_j$ are the average oxidation rate of $i$-th and $j$-th domains, respectively, $L_i(t)$ and $L_j(t)$ are perimeters of $i$-th and $j$-th domains, and $L(t)$ is the total boundary length of domains. To take account of a possibility of unsystematic domain boundary movement between domains with close orientations, a normally distributed random term ($U_{rnd}$) was introduced to the model.

Thus, the total area covered by moving domain boundaries at a certain time step can be calculated as

$$\Delta S(t) = \frac{\Delta t}{\gamma} \sum_{i=1}^{N} \sum_{j=i+1}^{N} \left| (U_{rnd} + U_i - U_j) \frac{L_i(t)L_j(t)}{L(t)} \right| \quad (6)$$

As far as termination of channels is a probabilistic process the fraction of terminated pores formed during $\Delta t$ can be derived from $\Delta S(t)$

$$n(t) = \Pi \frac{\Delta S(t)}{S} \quad (7)$$

where $\Pi$ is the probability of channel termination during domain boundary movement, and $S$ is the total area of the porous film.

This equation, however, is not directly applicable to evaluate the permeability of anodic alumina membranes, as it disregards the pore-blocking coordinate (see eq 1) and the multiple termination of pores. The latter is most appropriate for long-term anodization experiments, where several termination/splitting events can occur for a single channel. To consider a probability of multiple termination events for the same channel at different moments of oxidation (one under another), an additional normalization term reflecting permeable pore fraction, $(1 - N_t)$, should be introduced to the permeance calculations

$$n(t) = \Pi \frac{\Delta S(t)}{S}(1 - N_t),\ N_t = \sum_{\tau=0}^{t} n(\tau) \quad (8)$$

Thus the quantity of the "effective" dead-ended pores should be calculated recurrently, with the initial quantity of effective dead-ended channels equal to that formed in the upper layer.

Knowing the number of pores terminated at every time step, we can now derive a total membrane permeance using eq 1, by the following expression

$$P = \sum_{t=0}^{t_{fin}} p_{branch}(t)n(t)(1 - N_{t..t_{fin}}) + \frac{F}{H}(1 - N_{0..t_{fin}}) = \sum_{t=0}^{t_{fin}} \frac{F(H - h(t))}{(H + h(t))\cdot H} n(t)(1 - N_{t..t_{fin}}) + \frac{F}{H}(1 - N_{0..t_{fin}}) \quad (9)$$

where $N_{t..t_{fin}} = \sum_{\tau=t}^{t_{fin}} n(\tau)$ is the fraction of pores terminated from moment $t$ till the end of oxidation and $(1 - N_{0..t_{fin}}) = (1 - \sum_{\tau=0}^{t_{fin}} n(\tau))$ is the total fraction of nonblocked pores, which go straight from the top to the bottom of the membrane. Here, the first summand corresponds to the contribution of branches from straight channels, and the second summand reflects that of nonblocked pores.

Taking into account the nearly constant oxidation rate of aluminum in long-term oxidation experiments, eq 9 can be written in terms of membrane thickness

$$P = \sum_{h=0}^{H} \frac{F(H - h)}{(H + h)H} n(h)(1 - N_{h..H}) + \frac{F}{H}(1 - N_{0,H}) \quad (10)$$

where $N_{h..H}$ corresponds to the fraction of pores terminated from coordinate $h$ to the end of the membrane, and $(1 - N_{0,H})$ is the fraction of nonblocked pores.

The proposed model was used to fit experimental data on permeances of AAO membranes. The numerical simulations were carried out for the system of $1 \times 10^5$ pores with a constant diameter of 40 nm. Nucleation of pores at the initial stage of anodization was stated to comply with the oxidation rate, resulting in an initial distribution of pore orientations given by eq 4. The choice of nonrandom initial distribution of pore orientations was postulated in the model, to account for current instabilities developing on the aluminum surface during pore nucleation as a result of sample texture and surface relief.[5] Calculations were carried out with a step of ~1 $\mu$m thickness of the layer (which roughly corresponds to 0.5 h oxidation in 0.3 M $H_2C_2O_4$ at ~2 °C).[15] To calculate the permeance of membranes obtained by the two-step anodization technique, a preliminary calculation cycle was executed, to change the domain area distribution from the original one to that formed after the first anodization. Subsequently, $N_t$ was reduced to zero at the 100th step, corresponding to the duration of the first anodization of 48 h (membrane thickness of ~100 $\mu$m). Then the terminated pore density summation was started again.

The experimental values of permeance for AAO membranes, obtained by both single- and two-step anodization, are sufficiently fitted by the suggested model with parameters $k/\gamma$ = 0.25 $\mu$m/h, having a meaning of domain boundary movement rate coefficient; $\Pi$ = 1, and a standard deviation for $U_{rnd}$, $\sigma_{rnd}$ =

0.0365$k$. Corresponding relative permeance plots as a function of membrane thickness represent rather good agreement of experimental data with simulation results in a wide range of membrane thicknesses (Figure 3b).

According to the model, the specific perimeter of domains is maximal at the beginning of the first anodization, leading to the formation of a considerable quantity of branched and dead-ended channels. At longer anodization duration, the specific perimeter decreases substantially, with an increase in average domain size. All of these result in a decrease in the number of formed blocked channels. Moreover, the decrease in the domain's specific perimeter is accompanied by the decrease of the domain boundary movement speed, which entails more rare pore termination.

Despite a reduction in the pore termination rate with the increase in ordering of the AAO film, the total sum of $\sum_{t=0}^{t_{fin}} dS(t)/dt$ attains the total area of the porous membrane at ~50 h, and exceeds it roughly twice in long-term anodization experiments (~300 h). This means that moving domain boundaries sweep out the whole film area at least twice during the self-organization of the porous structure. This fact is definitely supported by experimental relative permeance values of ~0.2−0.3 achieved in long-term oxidation experiments, as compared to the theoretical minimum of 0.5$F$ derived from Fick's law for a membrane having every second pore terminated near the bottom (see eq 1). One should note that the obtained pore termination probability at domain boundaries, $\Pi = 1$, implies that any pore at the pore domain boundary should be branched. The total count of blocked channels gives a termination probability ranging from 1/25 $\mu m^{-1}$ at the initial stages to 1/300 $\mu m^{-1}$ in the steady state regime for oxidation conditions of 40 V at ~2 °C. These values were compared to electron microscopy observations of carbon replica grown within AAO channels by chemical vapor deposition (CVD, Figure 1f). The corresponding pore splitting density, found to be equal to 1/40 $\mu m^{-1}$, exceeds slightly the median of computed values, but agrees with the range, taking into account the low accuracy and high locality of microscopic methods.

To reveal the influence of duration of the first oxidation step on the AAO through porosity, we analyzed the series of samples obtained by two-step anodization with various preanodization durations (ranging from 3 to 48 h). Duration of the second anodization was equal to ca. 48 h for all membranes. One can easily see that an increase in preanodization duration (and thus sacrificial layer thickness) leads to the substantial growth of membrane permeance (Figure 4). A nearly 2-fold increase in permeance of the membrane is attained after a 10 h preanodization step. However, as a domain boundary movement occurs even after long-term anodization experiments, the permeance of the membrane will always be lower than the theoretical values calculated in a Knudsen flow approximation.

Theoretical fit of experimental data by the model, using parameters derived from the fitting of thickness dependence of relative permeance, represents rather a good agreement for the whole range of sacrificial oxide films thicknesses (Figure 4). This illustrates the flexibility of the proposed model, and its applicability for predicting the permeance of anodic alumina membranes. Moreover, a good agreement of experimental mass-transport data with the described model proves the mechanism of self-organization of porous structure, proposed earlier in ref 15.

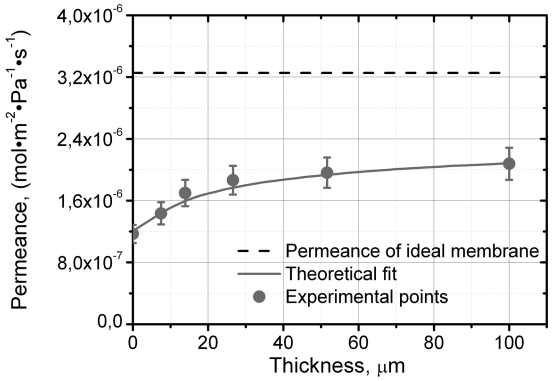


**Figure 4.** Permeance of 100 $\mu$m thick AAO membranes obtained by two-step anodization as a function of the thickness of the sacrificial oxide film formed on the first anodization stage. Experimental data are shown by circles and calculated values are given by the solid line. Permeance of an ideal membrane is shown by dashed line.

## CONCLUSIONS

In the present study, a comparative study of the structure and transport properties of porous aluminum oxide films, obtained by single- and two-step anodization, was carried out. Numerous termination and branching of channels, formed during anodic oxidation, are found to govern through porosity and permeability of AAO membranes. Utilization of a two-step anodization procedure allows an increase in the membrane permeance by a factor of 2. To provide a quantitative description of the pore termination process, a model of pore termination and splitting on moving domain boundaries is proposed. The presented approach describes reliably the experimental data on the permeance of AAO membranes and allows quick and easy prediction of the permeability of anodic alumina membranes of different thicknesses, synthesized by both single- and two-step anodization.

## AUTHOR INFORMATION

### Corresponding Author

*E-mail: di.petukhov@gmail.com. Phone:+7-495-9395248. Fax: +7-495-9390998.

### Notes

The authors declare no competing financial interest.

## ACKNOWLEDGMENTS

The work is partially supported by RF President Grant (Grant Nos. MK-7245.2012.3 and MD-4815.2013.3); the Russian Ministry of Education and Science (Grant 14.513.11.0017 and 16.552.11.7081); the Russian Foundation for Basic Research (Grant Nos. 11-03-00627, 12-03-00795 and 12-08-31562) and by M.V. Lomonosov Moscow State University Program of Development. Dmitrii Petukhov is also thankful to OPTEC LLC for the grant for project "Development of the anodic alumina membranes with branched porous structure for gas separation via capillary condensation".

## REFERENCES

(1) Keller, F.; Hunter, M. S.; Robinson, D. L. *J. Electrochem. Soc.* **1953**, *100*, 411−419.
(2) Masuda, H.; Fukuda, K. *Science* **1995**, *268*, 1466−1468.
(3) Li, F. Y.; Zhang, L.; Metzger, R. M. *Chem. Mater.* **1998**, *10*, 2470−2480.
(4) Han, X. Y.; Shen, W. Z. *J. Electroanal. Chem.* **2011**, *655*, 56−64.

(5) Sulka, G. D. In *Nanostructured Materials in Electrochemistry*; Eftekhari, A., Ed.; Wiley-VCH: Weinheim, Germany, 2008; pp 1−116.
(6) Sulka, G. D.; Brzozka, A.; Zaraska, L.; Jaskula, M. *Electrochim. Acta* **2010**, *55*, 4368−4376.
(7) Sulka, G. D.; Stroobants, S.; Moshchalkov, V.; Borghs, G.; Celis, J. P. *J. Electrochem. Soc.* **2002**, *149*, D97−D103.
(8) Choi, J.; Luo, Y.; Wehrspohn, R. B.; Hillebrand, R.; Schilling, J.; Gosele, U. *J. Appl. Phys.* **2003**, *94*, 4757−4762.
(9) Tsao, Y. C.; Sondergaard, T.; Skovsen, E.; Gurevich, L.; Pedersen, K.; Pedersen, T. G. *Opt. Express* **2013**, *21*, A84−A95.
(10) Lira, H. D. L.; Paterson, R. *J. Membr. Sci.* **2002**, *206*, 375−387.
(11) Peng Lee, K.; Mattia, D. *J. Membr. Sci.* **2013**, *435*, 52−61.
(12) Schwanbeck, H.; Schmidt, U. *Electrochim. Acta* **2000**, *45*, 4389−4398.
(13) Gorokh, G.; Mozalev, A.; Solovei, D.; Khatko, V.; Llobet, E.; Correig, X. *Electrochim. Acta* **2006**, *52*, 1771−1780.
(14) Wang, K. X.; Wang, Y. G.; Wang, Y. R.; Hosono, E.; Zhou, H. S. *J. Phys. Chem. C* **2009**, *113*, 1093−1097.
(15) Napolskii, K. S.; Roslyakov, I. V.; Eliseev, A. A.; Byelov, D. V.; Petukhov, A. V.; Grigoryeva, N. A.; Bouwman, W. G.; Lukashin, A. V.; Chumakov, A. P.; Grigoriev, S. V. *J. Phys. Chem. C* **2011**, *115*, 23726−23731.
(16) Kumar, S.; Sharma, S. K. *Superlattices Microstruct.* **2009**, *46*, 687−692.
(17) Lukatskaya, M. R.; Trusov, L. A.; Eliseev, A. A.; Lukashin, A. V.; Jansen, M.; Kazin, P. E.; Napolskii, K. S. *Chem. Commun.* **2011**, *47*, 2396−2398.
(18) Napolskii, K. S.; Roslyakov, I. V.; Eliseev, A. A.; Petukhov, D. I.; Lukashin, A. V.; Chen, S. F.; Liu, C. P.; Tsirlina, G. A. *Electrochim. Acta* **2011**, *56*, 2378−2384.
(19) Mozalev, A.; Magaino, S.; Imai, H. *Electrochim. Acta* **2001**, *46*, 2825−2834.
(20) Yampolsky, A. M. *Etching of Metals*; Metallurgy: Moscow, 1980; pp 129−134 (in Russian).
(21) Petukhov, D. I.; Napolskii, K. S.; Eliseev, A. A. *Nanotechnology* **2012**, *23*, 335601.
(22) Han, H.; Park, S. J.; Jang, J. S.; Ryu, H.; Kim, K. J.; Baik, S.; Lee, W. *ACS Appl. Mater. Interfaces* **2013**, *5*, 3441−3448.
(23) Lillo, M.; Losic, D. *J. Membr. Sci.* **2009**, *327*, 11−17.
(24) Lee, K. P.; Leese, H.; Mattia, D. *Nanoscale* **2012**, *4*, 2621−2627.
(25) Napolskii, K. S.; Roslyakov, I. V.; Romanchuk, A. Y.; Kapitanova, O. O.; Mankevich, A. S.; Lebedev, V. A.; Eliseev, A. A. *J. Mater. Chem.* **2012**, *22*, 11922−11926.